Engineering 2015, 1(1): 124–130
DOI 10.15302/J-ENG-2015013

Research
3D Printing—Article

Dual-Material Electron Beam Selective Melting: Hardware Development and Validation Studies

Chao Guo[1, 2, 3#], Wenjun Ge[1, 2, 3#], Feng Lin[1, 2, 3*]

ABSTRACT Electron beam selective melting (EBSM) is an additive manufacturing technique that directly fabricates three-dimensional parts in a layerwise fashion by using an electron beam to scan and melt metal powder. In recent years, EBSM has been successfully used in the additive manufacturing of a variety of materials. Previous research focused on the EBSM process of a single material. In this study, a novel EBSM process capable of building a gradient structure with dual metal materials was developed, and a powder-supplying method based on vibration was put forward. Two different powders can be supplied individually and then mixed. Two materials were used in this study: Ti6Al4V powder and Ti47Al2Cr2Nb powder. Ti6Al4V has excellent strength and plasticity at room temperature, while Ti47Al2Cr2Nb has excellent performance at high temperature, but is very brittle. A Ti6Al4V/Ti47Al2Cr2Nb gradient material was successfully fabricated by the developed system. The microstructures and chemical compositions were characterized by optical microscopy, scanning microscopy, and electron microprobe analysis. Results showed that the interface thickness was about 300 μm. The interface was free of cracks, and the chemical compositions exhibited a staircase-like change within the interface.

KEYWORDS additive manufacturing, electron beam, selective melting, gradient materials, titanium alloy, TiAl alloy

1 Introduction

Electron beam selective melting (EBSM) is an additive manufacturing (AM) process that utilizes an electron beam to fabricate three-dimensional objects layer by layer, based on a powder bed. In the EBSM process, the electron beam first preheats the substrate to a high temperature. Next, the building platform is lowered by an amount equal to the layer thickness, and a powder layer is spread onto the substrate. For each powder layer, the process includes two steps: ① preheating the powder layer and increasing the build temperature; and ② melting the cross-section. As the power density of an electron beam is extremely high, and as almost all of the electron beam energy can be absorbed by the metal materials, the EBSM process is favorable for manufacturing fully dense parts with high melting-point materials, such as Ti alloys. In addition, the build temperature during the process can be maintained at a high level (above 700 ℃), decreasing the thermal stress of built parts.

In recent years, EBSM has been successfully used in the AM of a variety of materials, including 316L stainless steel, Ti6Al4V, copper (Cu), Inconel 625 superalloy, cobalt (Co)-based superalloy, and TiAl alloy [1–5].

Previous research mainly focused on the EBSM of a single material. However, the application of EBSM requires further expansion, to allow this technology to be used to its full potential and capacity. One of the possible new applications of EBSM is the manufacturing of functional gradient materials (FGMs). FGMs were first proposed in the late 1980s. The main purpose of manufacturing FGMs is to optimize the distribution of mechanical properties in order to meet the requirements of complex working conditions. FGMs have been widely used in aerospace industries and in biological fields, where they are extremely important materials.

Many manufacturing methods have been employed to produce high-quality FGMs. These methods include powder metallurgy (PM), self-propagation high-temperature synthesis (SHS), plasma spraying, and AM technology [6]. In recent years, AM has been considered to be a promising manufacturing technology for fabricating FGMs. Banerjee et al. fabricated Ti8Al*x*V gradient materials using the laser metal deposition (LMD) process, in which the fraction of vanadium (V) gradually varied from 0 to 25% [7]. Sahasrabudhe et al. investigated the interface of a stainless steel and Ti6Al4V gradient material fabricated by the LMD process [8]. Wang

[1] Department of Mechanical Engineering, Tsinghua University, Beijing 100084, China; [2] Key Laboratory for Advanced Materials Processing Technology (Ministry of Education of China), Tsinghua University, Beijing 100084, China; [3] Biomanufacturing and Rapid Forming Technology Key Laboratory of Beijing, Tsinghua University, Beijing 100084, China
* Correspondence author. E-mail: linfeng@tsinghua.edu.cn
# These authors contributed equally to this work.
Received 16 February 2015; received in revised form 25 March 2015; accepted 25 March 2015

et al. manufactured Ti/Ti6Al2ZrMoV and Ti6Al2ZrMoV/Ti47Al2.5VCr gradient materials by LMD, and conducted detailed research on the chemical compositions, microstructures, and mechanical properties of the gradient materials [9, 10]. Liu et al. fabricated a gradient material of stainless steel and copper by selective laser melting (SLM) [11].

Although AM methods were used to fabricate these FGMs, the researchers mainly focused on laser processes, such as LMD and SLM. However, there are two issues involved in the laser-based AM of gradient materials. First, the absorption of laser energy by different materials varies considerably. Therefore, as the material composition changes, the laser power needs to be adjusted in real time to maintain a consistent melting condition. The adjustment of the laser power increases the difficulty of process control. Second, the thermal stress during the laser process is high, resulting in cracks in the built parts, especially at the interface of two different materials. In Refs. [8] and [11], cracks were found at the interface of the gradient materials. Heat treatment such as high temperature aging is essential for laser-built parts, to decrease or eliminate the residual thermal stress [10].

The EBSM process is a promising technology for building gradient materials of better quality. The differences in absorption of electron beam energy between different materials are small, and the higher build temperature during EBSM reduces the risk of thermal stress cracks. However, no research on the EBSM of gradient materials has been reported to date. In this study, a novel EBSM process involving dual materials was developed. Two different powders were used to fabricate parts. The mixing ratio of each powder layer can be tailored, so that parts can be fabricated with a material that undergoes a gradual change. A Ti6Al4V/Ti47Al2Cr2Nb gradient material was successfully fabricated using EBSM in this study, and the microstructures and chemical compositions of the fabricated samples were analyzed.

2 Hardware development

An EBSM system with the capacity for dual-material processing was developed, and a powder-supplying method based on vibration was put forward. Two different powders can be supplied individually and then mixed. In order to prolong the spreading comb's lifetime and avoid comb-tooth breakage, a comb-inclined powder-spreading method was employed.

2.1 Powder-supplying method based on vibration

Vibration was used as the power source to supply the powder materials through contact friction. Figure 1 shows the principal model of the powder-supplying method. In the original state, as shown in Figure 1(a), a powder exit is formed between the vibration plate and the powder storage container. The powder flows out of the exit, keeping still on the vibration plate because of the balance between gravity and friction. In Figure 1(b), the vibration plate moves forward with acceleration a. The powder inside the storage container remains still, due to the powder pressure and the storage wall restriction. The powder outside the storage container moves along the vibration plate, as long as the internal friction coefficient of the powder and the static friction coefficient between the powder and the vibration plate are above a/g (where g is the gravity acceleration). The moving distance equals the vibration amplitude, A. The motion of the powder breaks the balance, so as a result, powder flows out of the storage container, re-establishing a balanced state as shown in Figure 1(c). In Figure 1(d), the vibration plate moves back, and the powder remains still because of the restriction of the storage wall. Therefore, the powder on the vibration plate moves a distance of A in a vibration cycle. If the vibration plate keeps working, the powder will continuously move on the vibration plate, generating a stable powder flow off the vibration plate. The powder-supplying rate increases with an increase of vibration amplitude, powder exit height, and the powder materials' flowability.

The powder supplier has no revolute pair, and thus is highly reliable in a dusty environment, and does not get stuck by powder particles. The powder-supplying rate can be changed by altering the vibration amplitude and the height of the powder exit.

2.2 Dual powders mixing in tailored proportion

Figure 2 is a schematic of the dual powders mixer. Two powder suppliers based on vibration are placed side by side, facing each other. A powder-mixing box is placed directly below the edges of the vibration plates, and a weight sensor is used to measure the weight of powder in the mixing box in real time. Once the powder weight reaches the desired value, the vibrator stops working. The two powders can be supplied into the mixing box individually and precisely in order to obtain a mixture with a tailored proportion. Next, as shown in Figure 3, the mixing box rotates back and forth, blending the two powders, and finally pours the mixture onto the working platform. The powder spreader pushes the powder onto the building tank, filling the space on the deposited layers.

Assuming that the powder layer thickness is Δh, the area of the building tank is S, and the volume fraction of powder A in the layer is ε_A, then the amount of powder A, m_A, and the

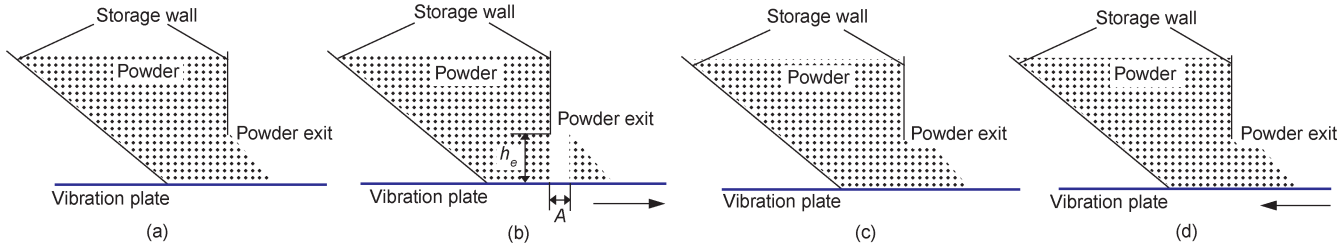

Figure 1. The schematics of the powder-supplying method. (a) Original state; (b) vibration plate moves forward, breaking the balance; (c) powder flows, re-balancing; (d) vibration plate moves back.

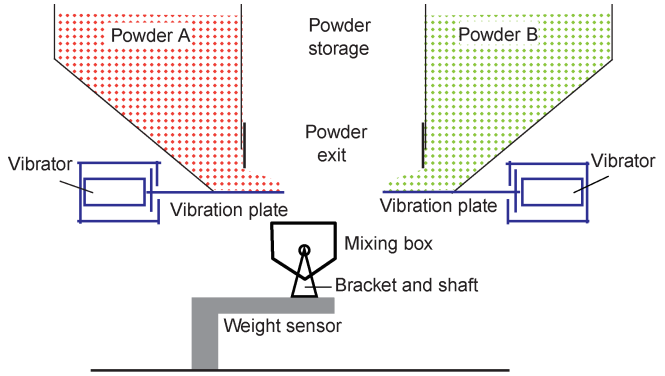

Figure 2. Supplying the two powders.

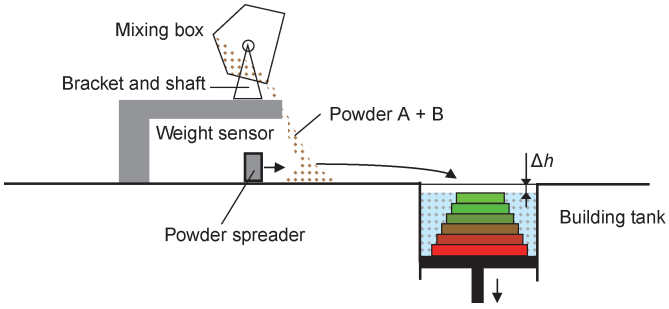

Figure 3. Mixing the two powders.

amount of powder B, m_B, can be calculated via Eqs. (1) and (2):

$$m_A = k\rho_A \Delta h S \varepsilon_A \quad (1)$$

$$m_B = k\rho_B \Delta h S (1-\varepsilon_A) \quad (2)$$

where $k > 1$, to compensate for the powder waste outside the building tank; ρ_A and ρ_B are the apparent densities of powders A and B; and for a process involving a single material, ε_A is set at 0 or 1.

2.3 Comb-inclined powder spreading

During EBSM, balling phenomena often occur, resulting in bumps on the deposited surface. When this happens, the powder spreader must scrape over the bump, as shown in Figure 4, which causes the comb teeth to bend. Vertical combs are commonly used in AM technologies that are based on a powder bed. Unfortunately, permanent deformation or breaking of the comb teeth often occurs. After scraping over the balling surface several times, irrecoverable deformation is found in some of the comb teeth. A deformed comb causes an uneven surface of the powder bed, and worsens the fabrication quality in the following deposition. In this study, instead of using a vertical comb, an inclined comb was utilized in order to reduce the risk of tooth deformation or breakage.

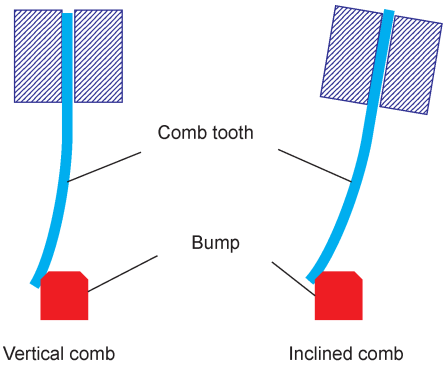

Figure 4. Vertical and inclined combs.

The maximum von Mises stress on a comb tooth scraping over a bump was computed by a finite element model, and the results are plotted in Figure 5. As the inclined angle increases, the maximum von Mises stress on the comb decreases greatly. For example, if the bump height is 0.3 mm, the maximum von Mises stress on a comb at a 25° inclined angle is only 20% of the stress on a vertical comb. A lower stress level means a lower risk of breakage for the comb tooth, and thus efficiently extends the comb lifetime.

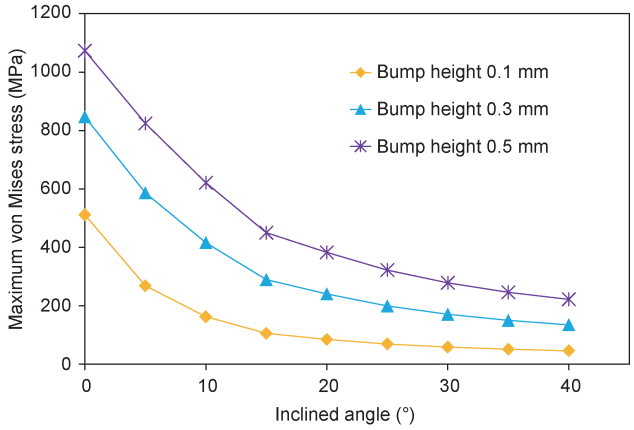

Figure 5. Maximum von Mises stress of comb tooth at different inclined angles.

3 Validation experiments

Two powders were used in this study: Ti6Al4V and Ti47Al-2Cr2Nb powder. These two powders were both gas-atomized and produced by the Northwest Institute for Non-Ferrous Metal Research, China. The size distribution of the Ti6Al4V powder was 50–260 μm, and the average particle size was about 125 μm. The chemical compositions (in weight percentages) were 6.46% aluminum (Al), 4.13% V, and the balance titanium (Ti). The size distribution of the Ti47Al2Cr2Nb powder was 40–150 μm. The Ti47Al2Cr2Nb powder had a chemical composition (in atomic percentages) of 46.51% Al, 0.02% niobium (Nb), 0.02% chromium (Cr), and the balance Ti. Ti6Al4V has excellent strength and plasticity at room temperature, while Ti47Al2Cr2Nb has excellent performance at high temperatures, but is very brittle. It is difficult for traditional processes to combine the plastic Ti6Al4V with the brittle Ti47Al2Cr2Nb.

Experiments were conducted on a team-developed EBSM system, shown in Figure 6. The maximum power of the electron beam is 3 kW (with an acceleration voltage of 60 kV and a maximum beam current of 50 mA). The previously described methods of a vibration-based supply, dual powders mixing, and comb-inclined spreading were applied to this system. The system contains two exchangeable building tanks with sizes of 100 mm × 100 mm × 100 mm and 250 mm × 250 mm × 250 mm. In this study, the smaller building tank was used to

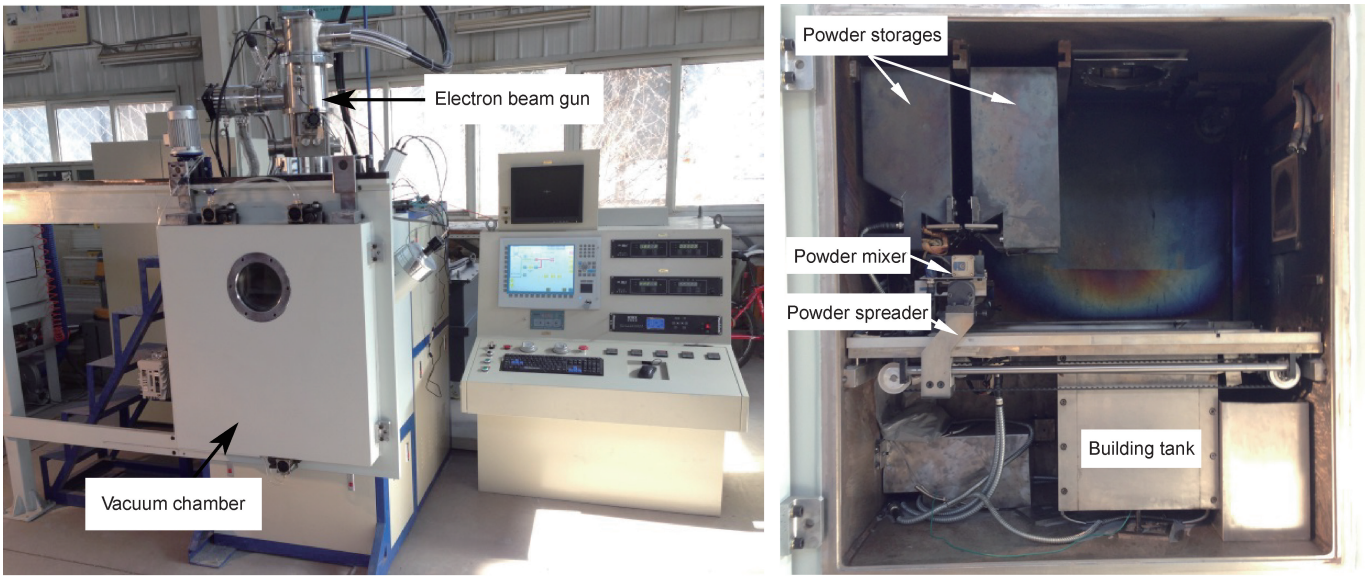

Figure 6. The dual-material EBSM system. (a) The system at a glance; (b) devices in the chamber.

fabricate small square samples.

A 316 L stainless steel substrate with a size of 90 mm × 90 mm × 10 mm was placed in the powder bed. Before depositing, the electron beam scanned the substrate for 20 min with a beam current of 15 mA, a defocusing current of 150 mA, a scanning line spacing of 1 mm, and a scanning velocity of 10 $m \cdot s^{-1}$. The layer thickness in this study was set at 100 μm. After one layer of powder was applied, the process included two steps: ① preheating the powder bed before melting; and ② melting through the powder layer and part of the previous layers. After fabrication, the samples remained in the vacuum chamber for approximately 4–5 h to cool down to room temperature.

The fabricated samples were cut along the deposition direction using electron-discharge machining, and were then mounted, ground, polished, and etched. Kroll's reagent was used to etch the samples. The microstructures of the samples were characterized by optical microscope (OM), scanning electron microscope (SEM) with backscattered electron (BSE) mode, X-ray diffraction (XRD), and transmission electron microscope (TEM).

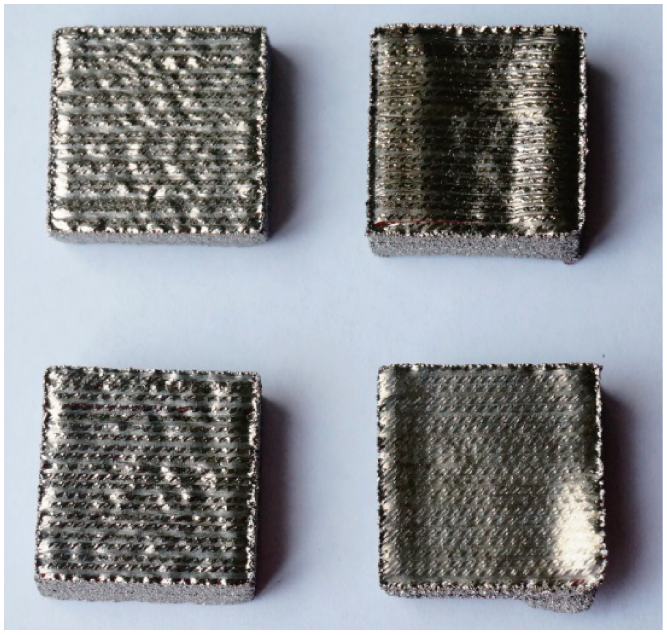

Figure 7. Square Ti6Al4V samples built by EBSM.

4 Results and discussion

The square Ti6Al4V samples built by EBSM are shown in Figure 7. The cross-section sizes of these samples are about 20 mm × 20 mm. In addition to Ti6Al4V, samples of Ti47Al-2Cr2Nb and Ti6Al4V/Ti47Al2Cr2Nb gradient materials were also fabricated. The analyses of their microstructures will be described later in this section.

4.1 Microstructures of Ti6Al4V samples

Figure 8 shows the microstructures of the Ti6Al4V fabricated by EBSM. As shown in Figure 8(a), columnar crystals parallel to the building direction can be seen. Within a distance of about 1 mm from the top, the microstructures were α′-martensite plates, as shown in Figure 8(b). Within the rest of the section, the microstructures were basket-weave structures with acicular α-phase grains (black) surrounded by the interfacial β-phase (white).

In their study, Hrabe and Quinn found that the microstructures did not vary with distance from the build plate [12]. In this study, however, a change of microstructures was observed. α′-martensite exists within a small distance from the top, and the α/β phase exists within the rest. This change provides evidence of the phase transformation during EBSM: For a given layer, the liquid phase transforms into the β phase several times because the beam penetration depth is greater than the layer thickness. Because of the very high cooling rate, the β phase first transforms into α′-martensite. Next, the α′-martensite decomposes into the α/β phase, because the layer is heated to the phase-transition temperature in the continued building cycle. Figure 9 shows the XRD patterns of the

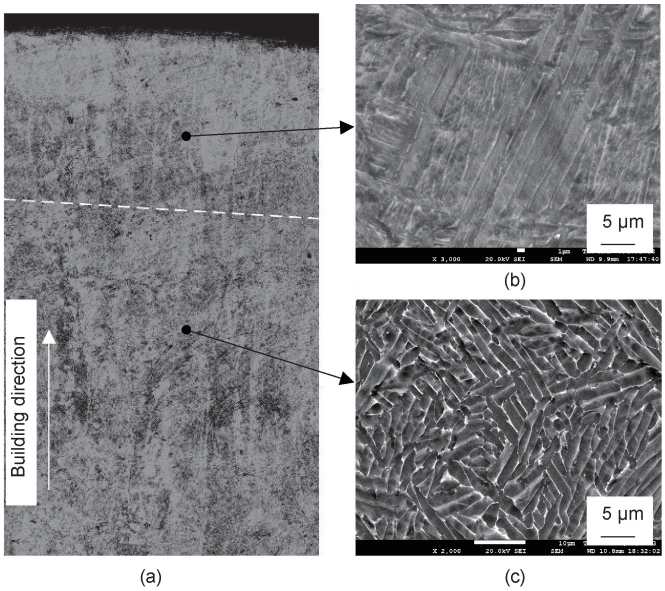

Figure 8. Microstructures of Ti6Al4V fabricated by EBSM. (a) Lower magnification by OM; (b) SEM picture of *α*′-martensite near the top; (c) SEM picture of the *α*/*β* phase away from the top.

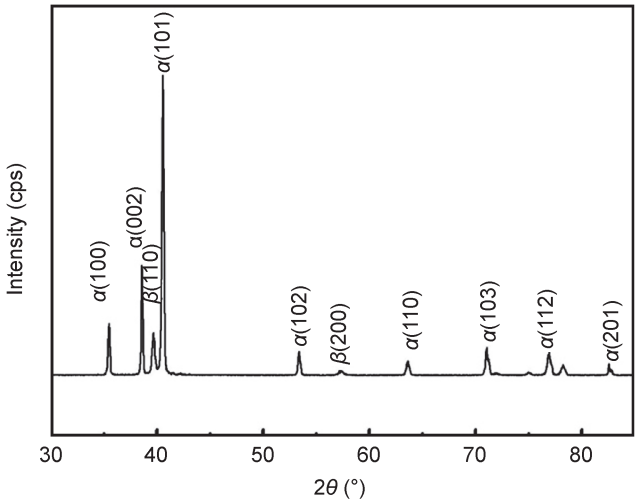

Figure 9. XRD pattern of EBSM-fabricated Ti6Al4V.

Ti6Al4V, which confirms the existence of the α and β phase. The residual α'-martensite within the top region in this study may relate to a lack of thermal insulation of the chamber. After building, the top region of the part quickly cools down and does not have enough time to finish decomposing from α'-martensite to the α/β phase.

4.2 Microstructures of Ti47Al2Cr2Nb samples

Figure 10 shows the BSE microstructures of the Ti47Al2Cr2Nb fabricated by EBSM. Dendritic morphology can be found in the top region of the sample. The angle between the main dendrite arm and the secondary dendrite arm is 90°, which proves that the primary solidification phase is the β phase. As seen in Figure 10, β dendrites grow along the building direction. According to the phase diagram, the solidification process is shown as follows:

$$L \rightarrow L+\beta \rightarrow \beta \rightarrow \beta+\alpha+\gamma \rightarrow \alpha \rightarrow \alpha+\gamma \rightarrow \alpha_2+\gamma$$

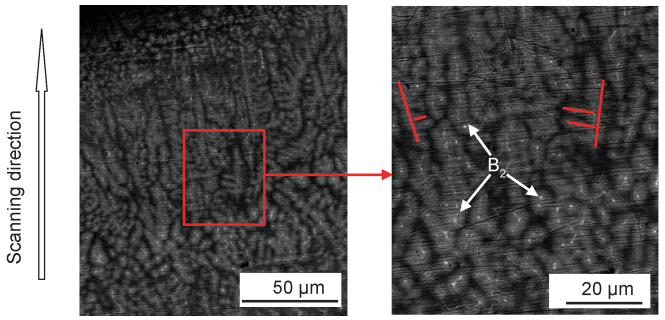

Figure 10. BSE microstructures of Ti47Al2Cr2Nb fabricated by EBSM.

The XRD patterns of the materials confirm that the main phase is γ and α_2, as shown in Figure 11. The grain size of the alloys with fully lamellar microstructure is 5–20 μm, which is considerably smaller than the typical grain in an as-cast lamellar structure (Figure 12). Figure 13 shows a TEM image of the full lamellar structure of the EBSM-fabricated Ti47Al2Cr2Nb. It can be seen that the thickness of the γ laths is about 0.5 μm and that of the α_2 laths is 0.1 μm. The γ slices and α_2 slices are arranged alternately.

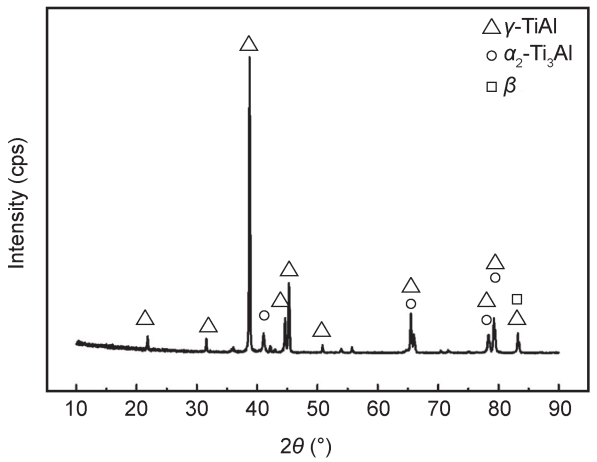

Figure 11. XRD pattern of EBSM-fabricated Ti47Al2Cr2Nb.

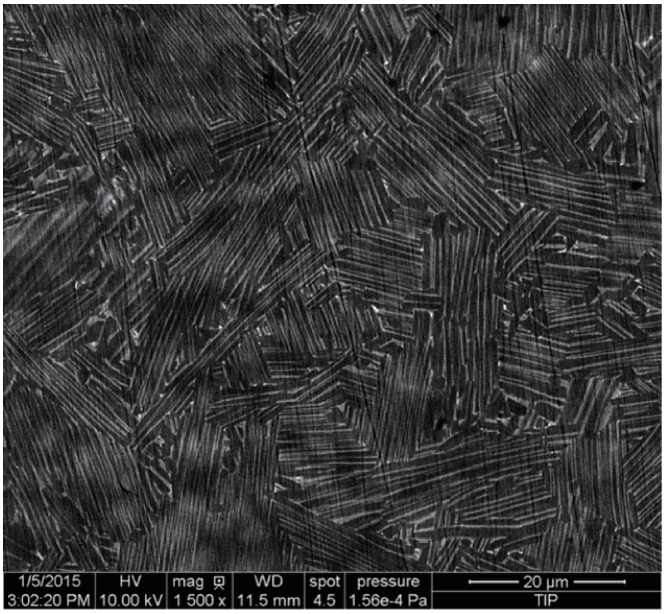

Figure 12. BSE image of EBSM-fabricated Ti47Al2Cr2Nb.

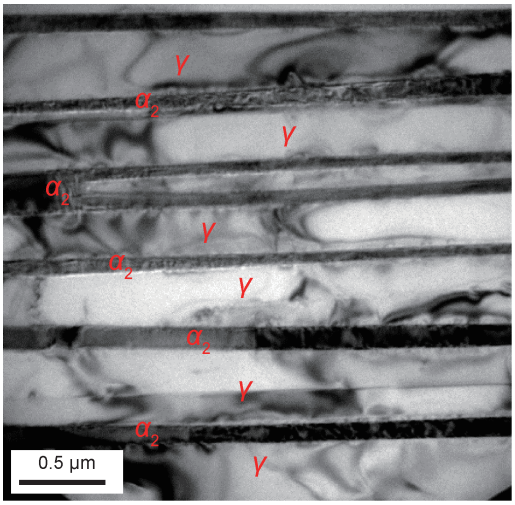

Figure 13. TEM image of the lamellar structure of the EBSM-fabricated Ti47Al2Cr2Nb.

4.3 Ti6Al4V/Ti47Al2Cr2Nb gradient structures

A Ti6Al4V/Ti47Al2Cr2Nb gradient material was successfully fabricated by EBSM. The material in the bottom 10 layers was Ti47Al2Cr2Nb, and the material in the top 20 layers was Ti6Al4V. Figure 14 shows the macrograph of the vertical section of the gradient material. No cracks were found in the interface.

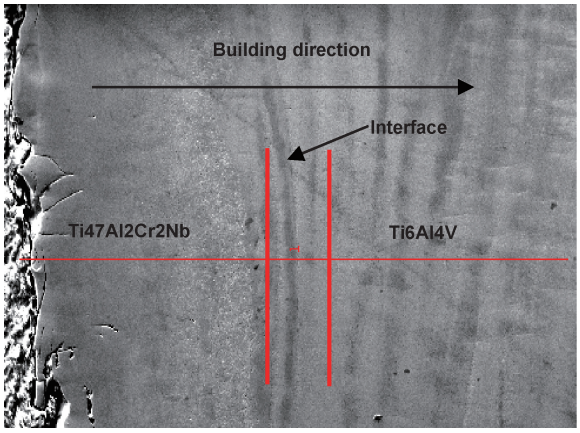

Figure 14. Macrograph of the vertical section of the gradient material.

A linear scan analysis using an electron probe micro-analyzer (EPMA) was employed to test the composition change in the building direction of the sample, and the results are shown in Figure 15. The results show that the interface thickness was about 300 μm. In the interface, the composition varied from Ti47Al2Cr2Nb to Ti6Al4V. Instead of a linear step change, two waves can be found in the content change curves of Ti and Al. The wave length is about 100 μm, which exactly equals the layer thickness. The presence of these waves demonstrates that the previous several layers were re-melted in the melting of the new layer, resulting in the staircase-like change.

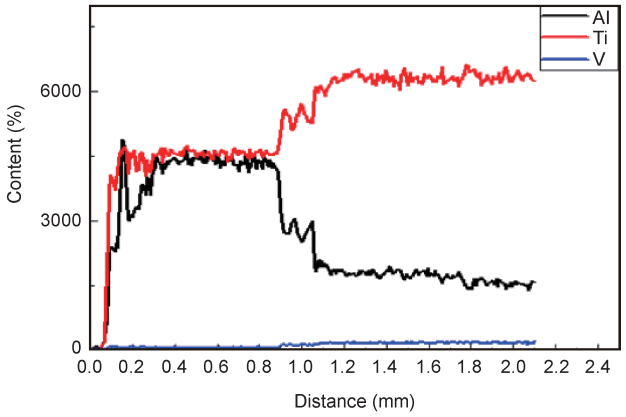

Figure 15. Composition change in the building direction of the sample.

Figure 16 shows the microstructures in a different region of the Ti6Al4V/Ti47Al2Cr2Nb gradient structure. Results show that the fully lamellar microstructure consisted of α_2-Ti_3Al, and that γ-TiAl was formed on the Ti47Al2Cr2Nb side, while a coarse basket-weave microstructure was formed on the Ti6Al4V side. The α phase thickness in the basket-weave microstructure was about 2 μm. In the top 5 layers at the Ti6Al4V side, the microstructure was needle-like α' lath martensite with a width of about 1 μm.

5 Conclusions

In this paper, a novel EBSM process capable of building a gradient structure with dual metal powders was developed. A powder-supplying method based on vibration was put forward. In this process, two different powders can be supplied individually and then mixed. In order to avoid yielding or breakage of the comb tooth, a low-deformation powder-

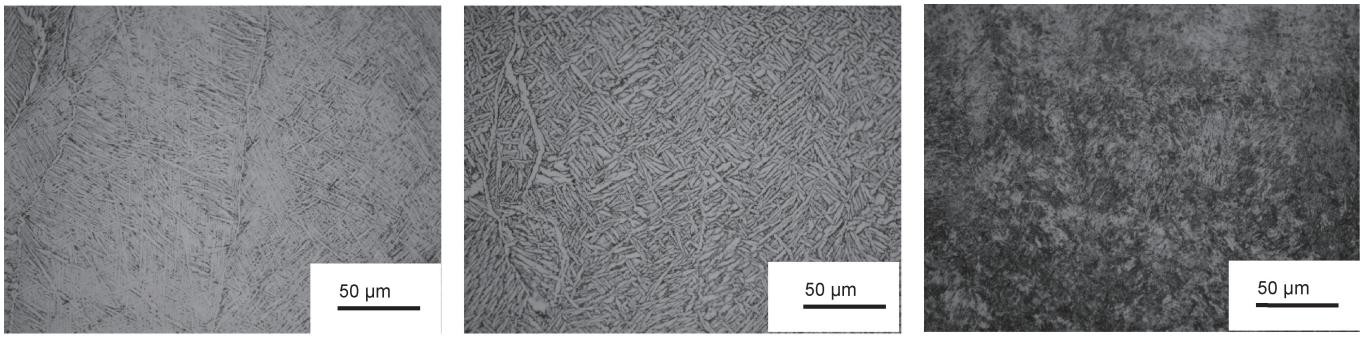

Figure 16. Microstructures of the gradient structure. (a) Top region of the Ti6Al4V side; (b) main region of the Ti6Al4V side; (c) Ti47Al2Cr2Nb side.

spreading device was designed.

Single-material samples were fabricated with Ti6Al4V and Ti47Al2Cr2Nb, respectively. For the Ti6Al4V, the microstructures were dominantly α/β phase, and α'-martensite was found within a small distance from the top. For the Ti47Al-2Cr2Nb, the microstructures were fully lamellar microstructures consisting of α_2-Ti_3Al and γ-TiAl.

A Ti6Al4V/Ti47Al2Cr2Nb gradient material was successfully fabricated. The interface thickness was about 300 μm. The interface was free of cracks, and the Ti element and Al element exhibited a staircase-like change within the interface.

Acknowledgements

The authors would like to acknowledge the funding of 2013 Beijing Science and Technology Development Project (D13110400300000 and D131100003013002).

Compliance with ethics guidelines

Chao Guo, Wenjun Ge, and Feng Lin declare that they have no conflict of interest or financial conflicts to disclose.

References

1. Y. N. Yan, H. B. Qi, F. Lin, W. He, H. R. Zhang, R. J. Zhang. Produced three-dimensional metal parts by electron beam selective melting. *Chin. J. Mech. Eng.*, 2007, 43(6): 87–92 (in Chinese)
2. D. Cormier, O. L. A. Harrysson, T. Mahale, H. A. West. Freeform fabrication of titanium aluminide via electron beam melting using prealloyed and blended powders. *Adv. Mater. Sci. Eng.*, 2008, 2007: 6822–6825
3. L. E. Murr, et al. Metal fabrication by additive manufacturing using laser and electron beam melting technologies. *J. Mater. Sci. Technol.*, 2012, 28(1): 1–14
4. L. E. Murr, et al. Microstructures of Rene 142 nickel-based superalloy fabricated by electron beam melting. *Acta Mater.*, 2013, 61(11): 4289–4296
5. S. H. Sun, Y. Koizumi, S. Kurosu, Y. P. Li, H. Matsumoto, A. Chiba. Build direction dependence of microstructure and high-temperature tensile property of Co-Cr-Mo alloy fabricated by electron beam melting. *Acta Mater.*, 2014, 64: 154–168
6. Y. Chen, C. Zeng, M. Yan. Research process of Ti base functional gradient materials. *Mater. Rev.*, 2012, 26(S1): 267–270 (in Chinese)
7. R. Banerjee, D. Bhattacharyya, P. C. Collins, G. B. Viswanathan, H. L. Fraser. Precipitation of grain boundary a in a laser deposited compositionally graded Ti-8Al-*x*V alloy—An orientation microscopy study. *Acta Mater.*, 2004, 52(2): 377–385
8. H. Sahasrabudhe, R. Harrison, C. Carpenter, A. Bandyopadhyay. Stainless steel to titanium bimetallic structure using LENS™. *Addit. Manuf.*, 2015, 5: 1–8
9. Y. Liang, X. Tian, Y. Zhu, J. Li, H. Wang. Compositional variation and microstructural evolution in laser additive manufactured Ti/Ti-6Al-2Zr-1Mo-1V graded structural material. *Mater. Sci. Eng. A*, 2014, 599: 242–246
10. H. P. Qu, P. Li, S. Q. Zhang, A. Li, H. M. Wang. Microstructure and mechanical property of laser melting deposition (LMD) Ti/TiAl structural gradient material. *Mater. Des.*, 2010, 31(1): 574–582
11. Z. H. Liu, D. Q. Zhang, S. L. Sing, C. K. Chua, L. E. Loh. Interfacial characterization of SLM parts in multi-material processing: Metallurgical diffusion between 316L stainless steel and C18400 copper alloy. *Mater. Charact.*, 2014, 94: 116–125
12. N. Hrabe, T. Quinn. Effects of processing on microstructure and mechanical properties of a titanium alloy (Ti-6Al-4V) fabricated using electron beam melting (EBM), part 1: Distance from build plate and part size. *Mater. Sci. Eng. A*, 2013, 573: 264–270